**2022 NDIA MICHIGAN CHAPTER**
**GROUND VEHICLE SYSTEMS ENGINEERING**
**AND TECHNOLOGY SYMPOSIUM**
**Modeling Technical Session**
**AUGUST 16-18, 2022, Novi, Michigan**

# A Modeling Methodology for the Analysis of Abradable Powder Piston Skirt Coatings

Daniel Nicklowitz and Harold Schock
Mid-Michigan Research
Andy Suman and Jim Lowe
Line2Line Coatings
Ai LeGrande Wood
DRC Engineering, Inc.

## Abstract

*Line2Line's patented abradable powder surface coatings are a mechanism by which clearance between mating components is reduced, and the tribological properties of the interacting surfaces can be improved. The following discussion presents the modeling efforts targeting the numerical analysis of abradable powder piston skirt coatings. This study employs the Cylinder-Kit Analysis System for Engines (CASE) by Mid-Michigan Research to model the performance enhancements offered by abradable powder coatings as applied to piston skirts. Two piston models were generated for the purposes of this analysis, one with the post-run stock reference geometry and coating, as supplied by the manufacturer, and the second having the Line2Line post-run coated geometry. The pistons modeled had been installed within two separate Cummins R2.8 L turbo diesel engines, both of which were subject to several hours of runtime. The primary finding of the current study is that the Line2Line abradable powder coated pistons, henceforth referred to as "APC" pistons, exhibited significantly less post-run clearance than the stock coated piston. The concept of "integrated skirt clearance" (ISC) is introduced. Integrated skirt clearance is a quantity that represents the volume between the piston skirt and cylinder liner. CASE is then employed to model the piston dynamics, frictional losses, and ring groove side wear associated with both the stock coated piston and the APC piston. The APC pistons are predicted to experience much less secondary motion than the stock coated piston. Less secondary motion results in lower ring groove side wear. Finally, a methodology is presented for the optimization of the piston skirt profile. The optimization employs both CASE and HEEDS by Siemen*

## Introduction

Throughout the last two decades, increasingly restrictive emissions regulations and the push toward vehicle electrification have forced engine manufacturers to seek unique solutions to improve the efficiency of the internal combustion engine. It is well understood that tighter piston skirt-to-liner clearances

will result in more desirable performance characteristics such as lower piston secondary motion, reduced noise, and improved combustion chamber sealing capabilities. Engineers are commonly faced with the competing interests of manufacturing costs and tight manufacturing tolerances. Tolerances are necessary to ensure adequate clearance in the cylinder kit assembly, thereby maintaining appropriate oil films while accounting for the cylinder-kit geometry changes resulting from thermal, inertial and pressure loadings. Each cylinder within an internal combustion engine will deform slightly different than its neighbors due to variations in thermal and mechanical loading throughout the engine block. This further complicates the optimization of piston-to-liner clearance. Abradable powder piston skirt coatings seek to provide a cost-effective and relatively simple solution to the consistent challenge of clearance control within the cylinder kit, among many other components which comprise the modern internal combustion engine.

While there has been extensive research on the optimization of piston geometry and the analysis of piston surface texture, few modeling efforts have emphasized the application of an abradable coating to a stock piston. Zhu et al. [1] formulated a piston dynamics model which employs the modified Reynold's equation proposed by Patir and Cheng [2,3] within the numerical solution of the hydrodynamic pressure between the piston skirt and cylinder liner. Gunelsu and Akalin [4] investigated the effects of skirt profile variations on piston secondary motion and friction. They then proposed a skirt profile which yielded a 17% reduction in power loss over the baseline design. Totaro et al. [5] performed an optimization of the skirt profile and proposed a final design that was not barrel-shaped yet yielded a 12% reduction in FMEP over the reference baseline design.

The findings of this paper add to those in a paper by Chowdhury [6], where the surface characteristics of a worn APC piston skirt were analyzed and compared with those of a stock piston. The surface topology and geometry of both a worn APC piston and a stock piston were modeled, and the results evaluated.

## Modeling Overview

The software utilized throughout this analysis is the Cylinder-kit Analysis System for Engines (CASE) by Mid-Michigan Research. CASE is a comprehensive cylinder kit analysis software package consisting of two programs: CASE-PISTON, and CASE-RING. These predict both piston and ring dynamics, losses, and wear.

### 1. Piston Dynamics Modeling

Within CASE, the piston axial dynamics are modeled as a traditional slider-crank mechanism. The crankshaft is assumed to rotate at a constant angular velocity, and the connecting rod is assumed to be rigid. Piston lateral dynamics constitute a highly non-linear problem that is solved iteratively considering the transverse forces acting on the piston due to combustion gas pressure, connecting rod orientation, boundary forces between the piston and cylinder liner, and hydrodynamic forces developed at the piston skirt-to-liner interface. The distribution of the piston forces also generates a moment about the piston pin, which causes the piston to rotate about the pin axis. This is referred to as secondary piston motion. The combination of piston lateral motion (secondary motion) and piston tilt contribute to undesirable vibration, noise, and losses due to the

collision of the piston and cylinder liner. This collision is also referred to as piston slap.

One of the dominating variables in the numerical simulations is the deformation characteristics of the piston. CASE is equipped with a complete finite element analysis package which employs linear tetrahedral elements. The thermal and mechanical deformations of the piston are material property dependent. The material properties of the piston employed in this study are detailed Table 1. The properties are taken as constant with no temperature dependence.

**Table 1. Piston Material Properties**

| | |
|---|---|
| **Modulus of Elasticity** | $\boldsymbol{75.0E9\ Pa}$ |
| **Poisson's Ratio** | 0.33 |
| **Mass Density** | $2670\ \frac{kg}{m^3}$ |
| **Conduction Coefficient** | $145\ \frac{W}{m \cdot K}$ |
| **Coefficient of Thermal Expansion** | $19.85E-6\ \frac{1}{K}$ |

The piston thermal deformation tends to be much larger in magnitude than the mechanical deformations caused by gas pressure loads, inertial loads, and skirt compliance. Due to the high frequency of an engine cycle, and therefore the relatively small amount of time for piston bulk heat transfer gradients, the piston temperature distribution and thermal load within CASE are assumed to be constant. The steady-state piston temperature distribution is determined by specifying temperature and convection boundary conditions at several regions on the piston. These regions include the piston crown, ring pack region, piston skirt region, piston under side, and pin hole region. The piston mesh includes an oil cooling gallery. The oil cooling gallery is assumed to be exposed to the same temperature and convection coefficient as the piston underside, providing additional cooling near the ring pack region. Experimental piston temperature data are not available. Therefore, a literature review was conducted [15-17], and the thermal boundary conditions were chosen such that the temperature distribution resembles the values reported in literature. The piston temperature distribution is shown in Figure 1, and the associated thermal deformation is shown in Figure 2.

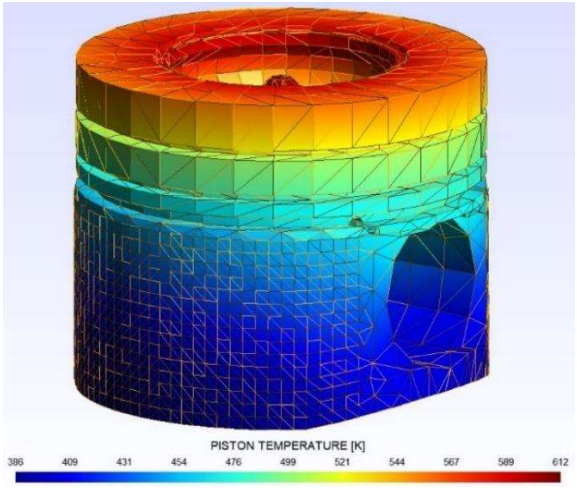


**Figure 1. Piston Temperature Distribution**

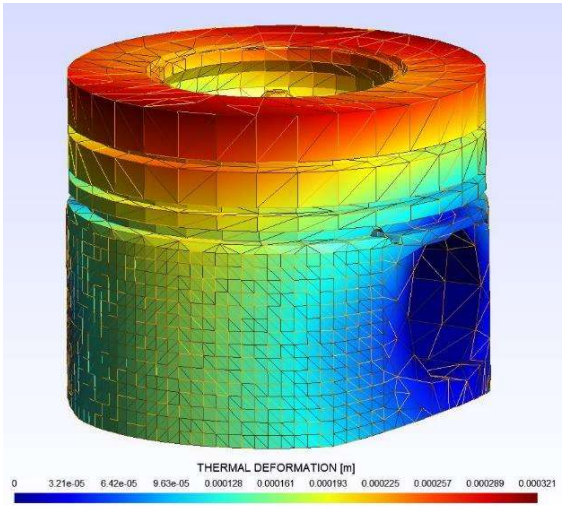

**Figure 2. Piston Thermal Deformation**

The piston deformations due to a unit body load and unit pressure load are each independently determined. Their magnitudes are appropriately scaled at each crank angle based on the piston acceleration and combustion gas pressure. The skirt deformation due to oil film and contact forces is determined via a skirt compliance matrix and the iterative solution of the hydrodynamic and boundary loads. The deformations are superimposed at each crank angle to determine the final piston geometry.

## 2. Surface Texture, Friction, and Wear Modeling

Boundary contact refers to the direct interaction of surface asperities without the separation of a lubricating film. The boundary contact load associated with two sliding surfaces is the dominating mechanism of friction and wear. In order to model the friction and wear characteristics of two lubricated sliding surfaces, here the piston and cylinder liner, the amount of transverse load supported by the oil film must be distinguished from the amount of transverse load supported by the surface asperities. Greenwood and Tripp [7] proposed one of the most widely accepted models for predicting the normal load supported by surface asperities. The Greenwood – Tripp model assumes a Gaussian distribution of surface asperity heights. It also assumes that only elastic contact occurs between the two surfaces.

$$p_a(h) = \frac{16\sqrt{2}\pi}{15}(\sigma_s\beta\eta)\ ^2E^*\sqrt{\frac{\sigma_s}{\beta}}F_{\frac{5}{2}}\left(\frac{h}{\sigma_s}\right) \qquad (1)$$

Where,

$p_a$ = Nominal contact pressure
$h$ = Nominal clearance between surfaces
$\sigma_s$ = Combined surface roughness
$\beta$ = Average summit radius
$\eta$ = Average area per summit
$E^* = \frac{1}{\left(\frac{1-\nu_1^2}{E_1}+\frac{1-\nu_2^2}{E_2}\right)}$ : Composite Elastic Modulus
$\nu_i$ = Poisson Ratio of Material *i*
$E_i$ = Elastic Modulus of Material *i*

$F_{\frac{5}{2}}$ requires the integration of the Gaussian distribution of asperity heights. The numerical integration of this term is computationally expensive. Thus, approximating functions have been introduced. Panayi [8] proposed an exponential approximation for the integration of the asperity heights, and this approximation is implemented in the current CASE-PISTON model. A sixth-order polynomial approximation proposed by Arcoumanis et al [9] is implemented in the CASE-RING analysis program.

Evaluation of eq (1) requires surface texture measurement data: surface mean summit radius, mean summit density (one over area per summit), and the surface roughness. These are readily measured through optical or stylus profilometry. Chowdhury showed that the surface texture measurements vary greatly across the face of a worn piston skirt, both axially and circumferentially [6].

A unique capability of CASE-PISTON is the ability to account for spatially varying surface texture inputs. A schematic of the spatially varying surface roughness of a worn APC piston is shown in Figure 3. The interested reader is referred to [6] for a more thorough analysis of the APC and stock piston surface textures.

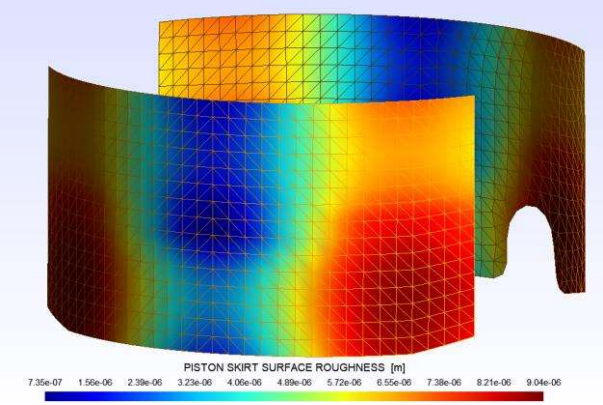


**Figure 3. Piston Skirt Surface Roughness Variation of APC Piston**

The abrasion of the Line2Line coating has a polishing effect on the skirt's surface. The regions of the piston skirt that experienced the highest wear have the lowest surface roughness post break-in. Figure 3 indicates that the APC piston experienced the most wear near the skirt center region, and the least wear near the lower outer circumferential locations. Figure 4 shows a magnified image of the APC piston skirt surface before and after break in. The post-run APC surface had numerous micron-sized pockets which are believed to improve the oil-retention properties of the piston skirt while simultaneous reducing the area of boundary contact. This detail is not currently accounted for in CASE-PISTON, although efforts are underway to implement models that capture this feature.


**Figure 4. APC Surface Texture (103X)**

Once the load carried by surface asperities between two interacting surfaces is known, the wear can be estimated. This is commonly done using Archard's model, which states that the wear is proportional to the load carried by surface asperities, the sliding distance between the two interacting surfaces, and a dimensionless wear coefficient; and inversely proportional to surface hardness.

$$\psi = k(\frac{W_a L}{H}) \quad (2)$$

Where,

$\psi$ = worn volume
k = wear coefficient
$W_a$ = asperity contact load
$L$ = relative sliding distance
$H$ = surface hardness

## Model Configuration

The geometrical simulation inputs were obtained via the direct measurement of the relevant engine components. Utilizing the piston geometry measurements, a CAD model of the piston was generated using Siemens NX, which was then meshed in Altair Hypermesh for use within the CASE-PISTON finite element model. The piston mesh is shown in Figure 5

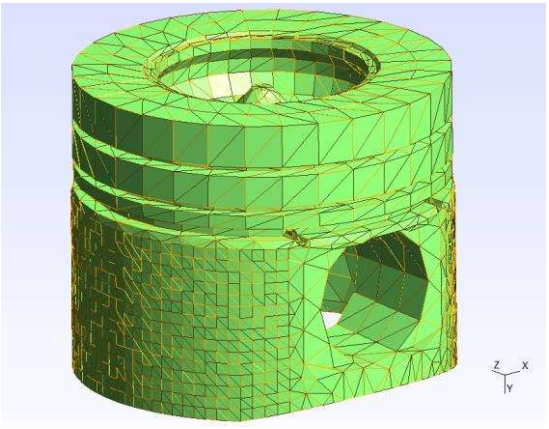

**Figure 5. Piston Mesh**

Combustion gas pressure data was obtained via experimental measurements using in-

cylinder pressure transducers and a CAS measurement system with an encoder resolution of 0.1 crank angle degrees. Data for 250 cycles of combustion gas pressure data were recorded at each operating condition. The pressure data was averaged over the 250 cycles and is shown in Figure 6.

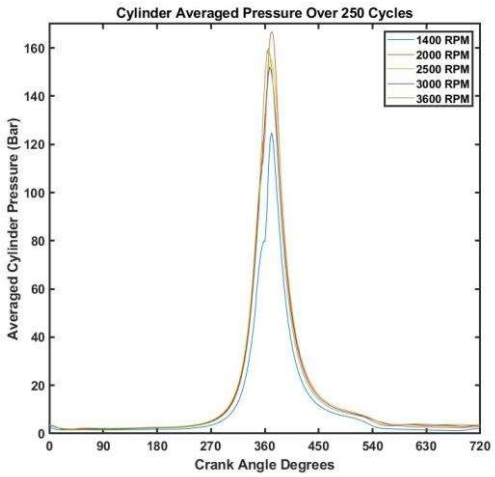


**Figure 6. Measured In-Cylinder Gas Pressure**

Experimental bulk combustion gas temperature and interior liner temperature data were not available. Therefore, a GT-Power R 2.8 engine model was configured and calibrated using experimental data and turbocharger maps supplied by the engine manufacturer. In-cylinder bulk gas temperature data were obtained via a thermal finite element analysis with GT Spaceclaim. A more detailed overview of the GT modeling theory was presented by Chowdhury [6]. A summary of the model configuration and specific relevant simulation conditions are shown in Figure 7 and Table 2 respectively.

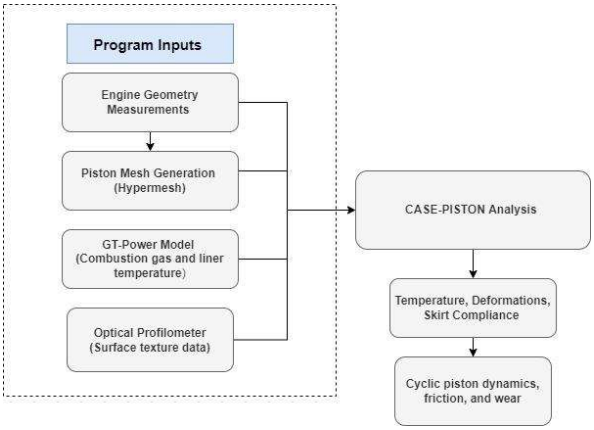


**Figure 7. Program Flowchart**

**Table 2. Engine Geometry**

The primary variable under investigation in the current study is the geometric difference

| Parameter | Value |
|---|---|
| **Engine Speed** | 2000 RPM |
| **Bore Diameter** | 94.25 mm (At Operating Temp.) |
| **Stock Piston Diameter** | 93.901 mm (Cold) |
| **APC Piston Diameter** | 93.957 mm (Cold) |
| **Stock Piston Ovality** | -0.3505 mm |
| **APC Piston Ovality** | -0.4267 mm |
| **Stroke** | 100 mm |
| **Compression Ratio** | 16.9 |

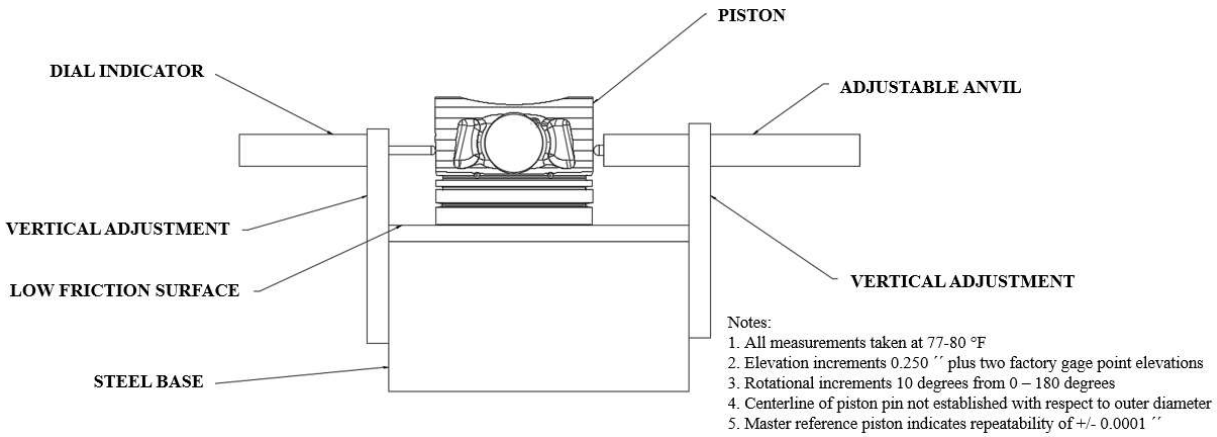


**Figure 8. Piston Measurement Configuration**

between the stock and APC piston skirts. These inputs are also supplied via physical measurements of post-run stock and APC pistons. Note that the stock piston includes the stock graphite coating. The post run stock graphite coating is accounted for in the piston measurement data. A measurement methodology has been developed using a fixed platform with a mounted analog dial indicator. A schematic of the measurement device is shown in Figure 8. Gage pins are used to calibrate the measurement device at the beginning of each measurement session. The piston rests on a low friction graphite platform during the measurements to ensure a high level of accuracy. A baseline piston is measured during every measurement session to ensure that the calibrated device is producing the same standard results between sessions. With this strategy, accuracies of +/- 0.1 thousandths of an inch (+/- 2.5 microns) are achieved. The post-run stock and APC piston diameter measurements are detailed in Figure 99 and Figure 1010 respectively.

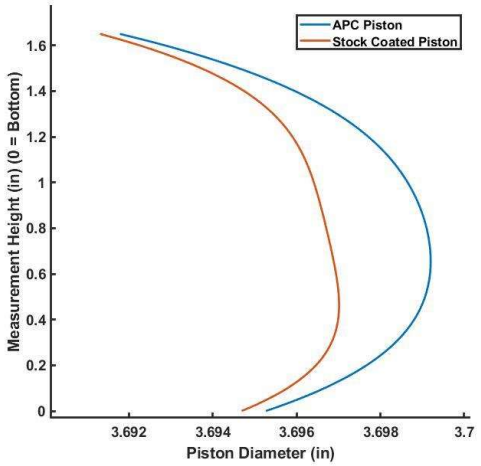


**Figure 9. Axial Stock vs. APC Piston Trace**

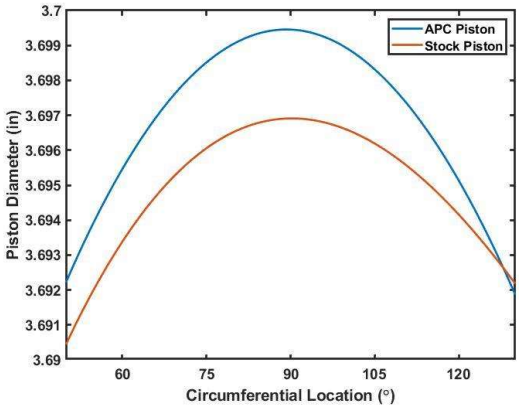


**Figure 10. Circumferential Stock vs. APC Piston Trace**

The axial piston measurement trace shown in Figure 99 was measured at the 90-degree circumferential location, or along the skirt's center. The circumferential trace shown in Figure 1010 was taken 0.632'' from the skirt bottom, which is the height of the gauge point where the piston would typically be measured with a standard set of micrometers. While axial and circumferential measurements were taken at several other locations, the two shown in the previous figures are generally representative of the stock vs. APC piston geometries for the current comparative study. Figure 9 and Figure 10 indicate the post run APC piston has significantly less clearance in both the axial and circumferential directions. The post-run APC piston diameter is also slightly more symmetrical about the 90-degree circumferential location as compared to the stock piston. A visualization of the pre and post run APC piston as compared to the post run stock piston is shown in Figure 111.

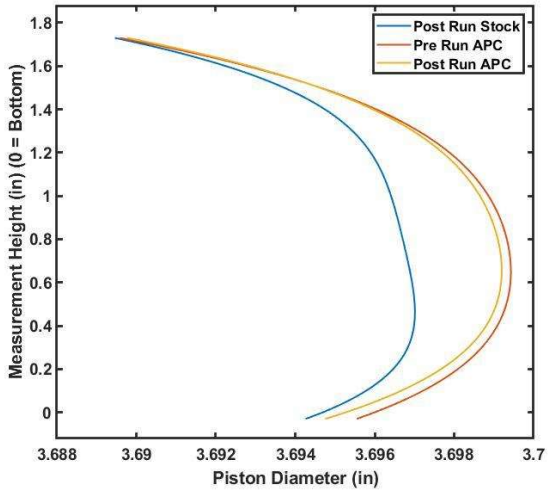


**Figure 11. Pre and Post Run Piston Diameters**

The total volume between the piston skirt and cylinder liner is referred to as the integrated skirt clearance (ISC). The ISC is the envelope of space surrounding the piston where secondary motion can occur. Effectively reducing the ISC can limit the amplitude of undesirable piston motion and the degree of oil piercing potential of the piston assembly. The post run APC piston has a significantly smaller ISC than the stock coated piston. A quantification of the cold ISC is generated by numerically integrating the clearances at several measurement locations around the skirt while assuming a stock 94 mm bore. The ISC calculation is summarized in Table 3.

**Table 3. Cold Integrated Skirt Clearance**

| **Piston** | **ISC ($mm^3$)** |
|---|---|
| **Stock** | 588.741 |
| **APC** | 482.627 |

Clearances above 0.02 inches were assumed to be off the skirt and were therefore filtered out of the ISC calculation. Efforts are underway to utilize CASE-PISTON to calculate the ISC at each crank angle while accounting for the thermal and mechanical loading of the piston and deformation of the cylinder liner.

Using the axial piston trace, a radial skirt profile input is generated for CASE-PISTON. The circumferential trace is used to generate the ovality input as displayed in Table 2. The piston ovality is a single input parameter that describes the difference between the piston diameter in the thrust plane, and the piston diameter along the pin axis. Piston ovality is often described by a double ellipse equation, which is represented by an ellipse formula of the form

$$\delta_o = \frac{1}{4\left[\alpha\left(1-\cos 2\theta_p\right) - \beta\left(1-\cos 4\theta_p\right)\right]}$$

Where $\delta_o$ is the difference between the piston nominal radius and the actual piston radius at a circumferential location $\theta_p$, which is measured from the thrust plane. The quantities α and β are independent

coefficients, which are solved for using the piston circumferential trace shown in Figure 1010. At operating temperature, the piston skirt profile and piston diameter change considerably due to thermal expansion. The thermal gradient of the piston is such that the expansion is greater near the top of the skirt than the bottom. The larger expansion near the top region of the skirt justifies the smaller diameter at this axial location shown in Figure 9. A comparison of the stock piston radius before and after thermal expansion is shown in Figure 12.

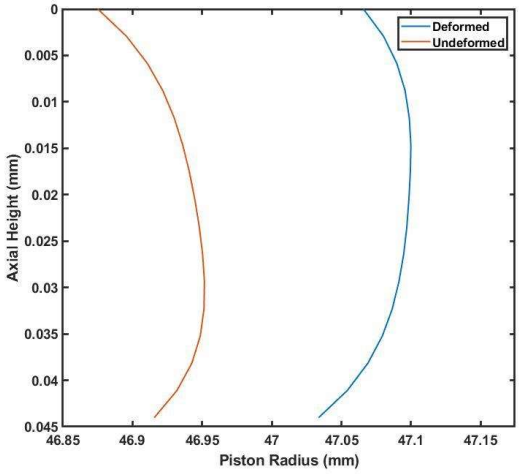


**Figure 12. Stock Piston Radius Before and After Thermal Expansion**

**The radial skirt profile is calculated as the distance from the nominal radius at each axial location. The nominal piston radius is typically taken as the maximum radius of the piston skirt. The piston skirt profile of the stock piston before and after thermal expansion is detailed in**

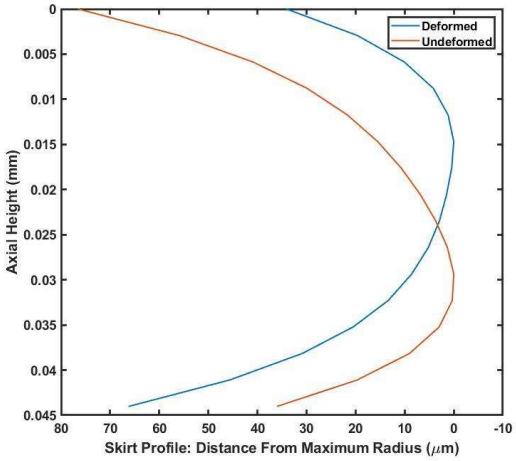


Figure 133.

**Table 4. Piston Run Conditions**

| Piston History | Stock \| APC |
|---|---|
| Runtime | 200 hours \| 20 hours |
| Type (Measured/Modeled) | Measured \| Measured |
| Maximum Load | 120% torque \| 110% torque |
| Measurement Type | Post Run/Cold \| Post Run/Cold |
| Break-in | None \| Standardized |

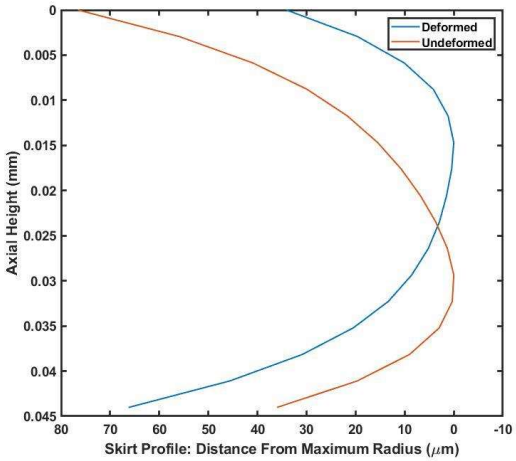

**Figure 13. Stock Skirt Profile Before and After Thermal Expansion**

Piston run conditions are detailed in Table 4. It must be noted that the stock and APC pistons were subject to different engine tests. It is believed that each piston had approximately reached its final run-in geometry. The abradable coating was significantly softer than the stock coating and was able to be removed easily by hand using a fine emery cloth. The 20-hour standardized break-in procedure is intended to wear the APC piston to its final geometry. In the coming phase of the project, an engine with APC pistons and a stock engine will be tested under identical conditions.

## Piston Dynamics Modeling Results

The piston transverse position in the cylinder is described by several eccentricities which represent the lateral position in the cylinder liner at different axial locations on the piston. In general, the eccentricity at the piston pin height and the piston tilt angle are sufficient to characterize the secondary motion. These two predicted quantities are shown in Figure 144 and Figure 155 respectively.

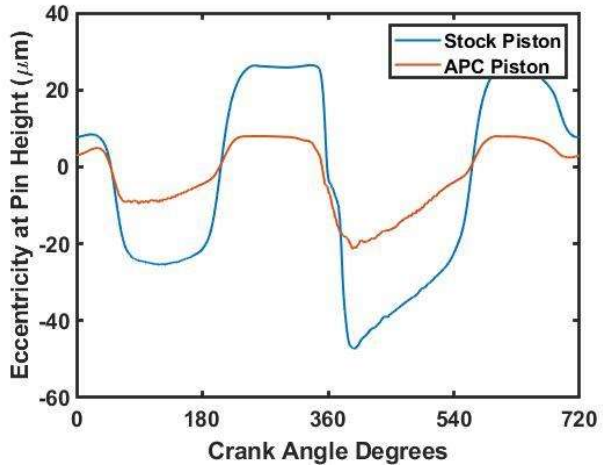


**Figure 14. Eccentricity at Pin Height**

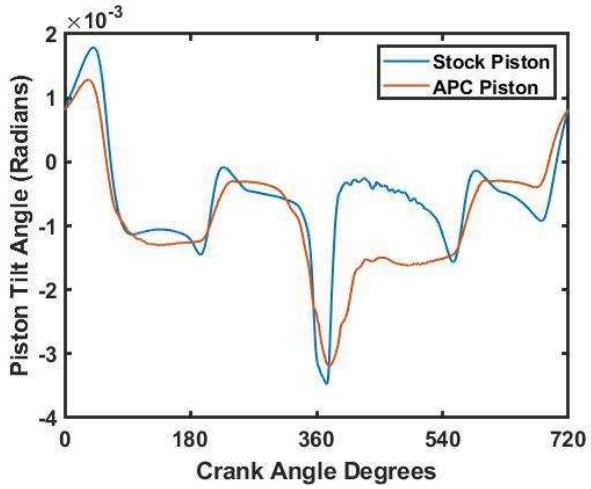


**Figure 15. Piston Tilt**

The APC piston has a significantly smaller ISC than the stock piston. The tighter clearances yield a significant reduction in secondary motion and piston tilt. This translates to less engine noise, vibration, and improved user comfort. Lower secondary motion and piston tilt also contribute to lower ring groove side wear, as detailed in the following section.

## Ring Groove Side Wear Results

Equation 2 states that the worn volume of two interacting surfaces is proportional to the relative motion between the two surfaces. There are several mechanisms of relative motion between the ring and piston including ring circumferential motion, radial motion due to bore distortion, ring twist, and secondary motion. Ring circumferential motion is not currently implemented in the CASE-RING model. Effects due to bore distortion are not present in this analysis since the cylinder bore is assumed to be uniform in diameter. Hence, the two modes of relative motion between the ring and groove in the present study are piston secondary motion and ring twist. Out of these two, the piston secondary motion typically causes more relative sliding

than ring twist. Therefore, the reduced secondary motion detailed in the previous section is expected to yield significantly reduced ring groove side wear. This effect is detailed in Figure 166 through Figure 199.

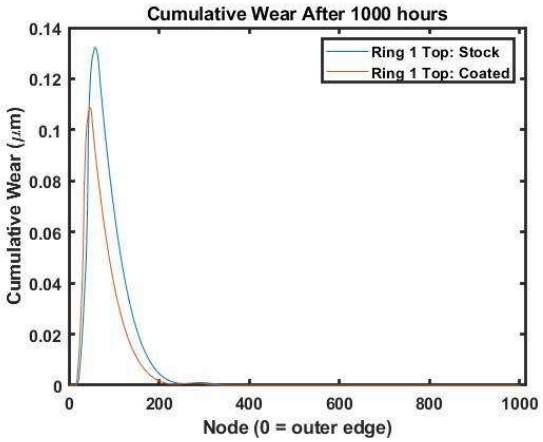


**Figure 16. Ring 1 Top Wear**

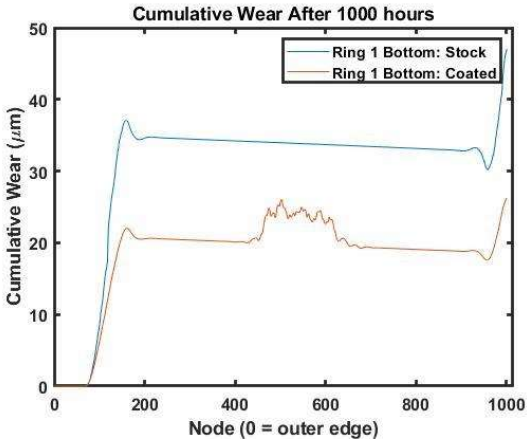


**Figure 17. Ring 1 Bottom Wear**

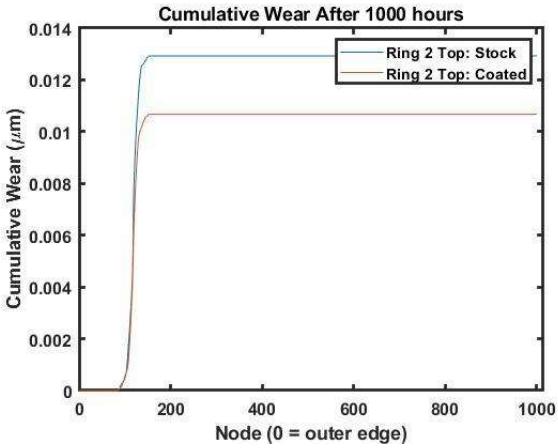


**Figure 18. Ring 2 Top Wear**

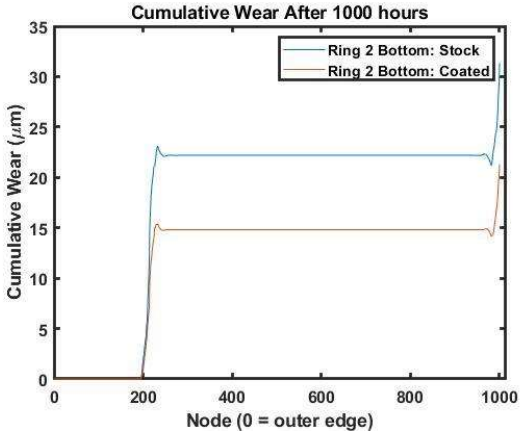


**Figure 19. Ring 2 Bottom Wear**

The reduced secondary motion associated with the APC piston is expected to yield a significant reduction in ring wear. This reduction in ring wear is expected to lead to better ring sealing capabilities, reduced blow-by, and extended durability. The reduced secondary motion and piston tilt is also expected to improve the sealing of the combustion chamber, although the magnitude of this effect still needs to be investigated. Efforts are underway to implement these capabilities within CASE-RING.

## A Skirt Profile Optimization Methodology Employing CASE and HEEDS

To investigate the geometric features of the piston skirt profile which lead to reduced frictional losses, an optimization methodology has been developed employing CASE-PISTON by Mid-Michigan Research and HEEDS by Siemens. For the purposes of this optimization, the objective was chosen to minimize the average cyclic friction power loss. This output is the product of frictional force and velocity averaged over the engine cycle. The hypothesis is that the abradable powder coating will wear in such a way to minimize the asperity contact between the piston skirt and cylinder liner, thus achieving a geometry that minimizes boundary contact. In order to limit the number of variables within the design space of the optimization, CASE-PISTON accepts five input parameters ($a_0$ $through$ $a_4$) which are fit with a fourth-order polynomial. The parameters describing the skirt profile are detailed in Figure 2020.

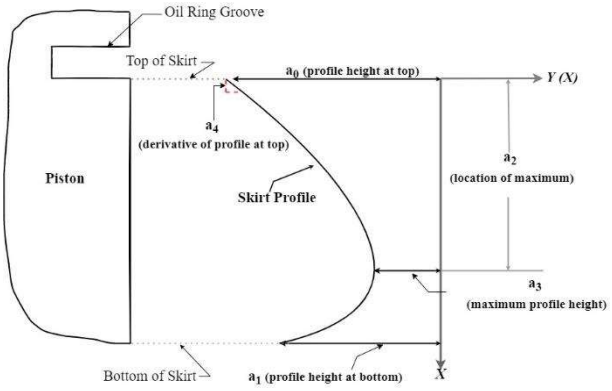


**Figure 20. Skirt Profile Polynomial Parameters**

Two constraints are needed to ensure that the profile maintains a barrel shape. Noting that the skirt profile is represented by a fourth order polynomial, the first constraint is that the discriminant of the first derivative of the skirt profile must be less than zero. Formally, this ensures that the first derivative of the skirt profile (a third order polynomial) has only one real root (and two complex roots). The single real root forces only a single stationary point, where the skirt profile slope is equal to zero. An additional constraint is required to ensure that the single stationary point is a maximum. To achieve this, the second derivative of the skirt profile is forced to be less than zero at the skirt bottom. This ensures the concavity of the function to be such that the stationary point is a maximum. The optimization problem is formally defined as

Find $\boldsymbol{a} = \{a_0, a_1, a_2, a_3, a_4\} \in \mathbb{R}^5$ that

Minimize:

$$\dot{W}_{f_{avg}} = \frac{1}{720}\int_0^{720} \left[F_{f_{Hyd}}(h(\delta),\theta) + F_{f_{Asp}}(h(\delta),\theta)\right] V_{axial}(\theta)\, d\theta$$

Subject to:

$$\boldsymbol{a_{min}} < \boldsymbol{a} < \boldsymbol{a_{max}},$$
$$g_1(\boldsymbol{a}) = D_3\left(\delta'(x_s)\right) \leq 0,$$
$$g_2(\boldsymbol{a}) = \delta''(x_{sb}) \leq 0$$

Where,

$\dot{W}_{f_{avg}}$: Average friction power loss
$F_{f_{Hyd}}$: Hydrodynamic friction force
$F_{f_{Asp}}$: Boundary friction force
$h$: Skirt-to-liner clearance
$\delta$: Skirt profile height
$V_{axial}$: Axial piston velocity
$\theta$: Crank angle
$D_3$: Discriminant
$x_s$: Skirt axial location
$x_{sb}$: Axial location of the skirt bottom
$g_i(\boldsymbol{a})$: Constraint on $\boldsymbol{a}$

The bounds of the optimization are chosen such that the optimized piston skirt profile is always greater than the stock piston skirt profile, as the abradable powder coating adds material to the piston skirt. To reinforce this restriction, an additional constraint was placed within the executable, which stops the iteration if any point on the skirt surface is less than the stock skirt. It must also be noted that the optimization study was conducted with a 94.3 mm bore, which is 50 microns larger than the bore diameter used in the cyclic piston dynamics results presented earlier. This discrepancy arises from the computational time required to conduct the optimization and the continual improvement of the simulation inputs. As the simulation inputs are improved, further optimization studies will be conducted.

HEEDS is configured to run approximately 350 test cases at several different engine operating speeds and loads. In order to reduce the computational time required for each iteration, the mesh density has been significantly decreased. The mesh utilized in the optimization is shown in Figure 21.

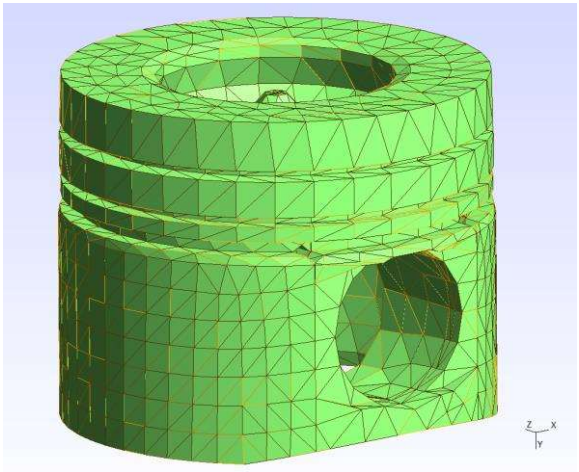

**Figure 21. Coarse Mesh for Optimization**

While the density of the piston mesh used in the profile optimization was coarse, the mesh size was determined to be sufficient for a comparative analysis. A brief mesh sensitivity study is presented in appendix A.

While the engine speed and load were varied during the optimization study, several inputs were held constant across the engine operating conditions. The inputs that were held constant include the piston temperature distribution, the liner temperature, and the bore diameter. Future appropriate modifications will be made to improve this study. The optimized profiles at 2000 RPM and 3600 RPM are shown in Figure 22, and the optimization results are quantified in Table 5.

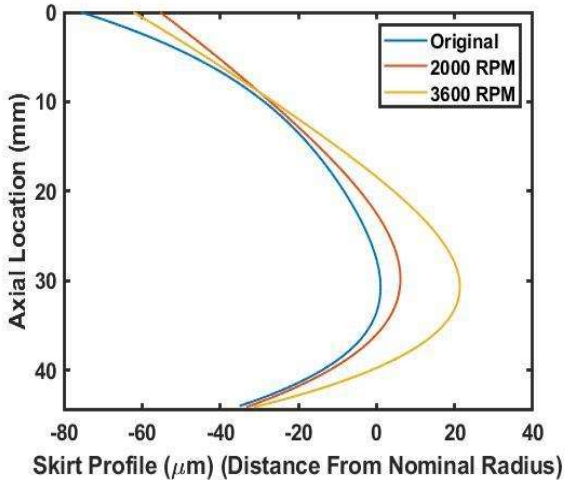


**Figure 22. Optimized vs. Original Skirt Profile**

**Table 5. Power Loss Optimization Results**

| RPM | Original | Optimized | % Gain |
|---|---|---|---|
| **2000** | 468.89 W | 417.96 W | 10.86 % |
| **3600** | 1132.4 W | 909.05 W | 19.72 % |

A breakdown of the friction power loss prediction into its hydrodynamic shear and boundary friction components is shown in

Table 6.

**Table 6. Power Loss Breakdown**

| CONFIGURATION | HYDRODYNAMIC | BOUNDARY |
|---|---|---|
| 2000 RPM ORIGINAL | 104.83 W | 364.06 W |
| 3600 RPM ORIGINAL | 364.06 W | 759.92 W |
| 2000 RPM OPTIMIZED | 105.46 W | 312.50 W |
| 3600 RPM OPTIMIZED | 366.20 W | 542.88 W |

The predicted power loss results shown in Table 5 are in approximate agreement with the experimentally measured results. At 2000 RPM, in cylinder pressure data and BMEP data were utilized to calculate an experimental FMEP value for the stock engine of approximately 2.25 Bar. The FMEP values are related to power loss by

$$FMEP\ (psi) = \frac{Power\ loss\,(hp) \times n_R \times 396{,}000}{V_d\,(in^3) \times N\left(\frac{rev}{\min}\right)}$$

Where,

$FMEP: Friction\ Mean\ Effective\ Pressure$
$n_R: Crankshaft\ revs.per\ power\ stroke$
$V_d: Displacement\ Volume$
$N: Engine\ Speed$

Solving the above equation for power loss yields a total engine power loss of 14.08 HP, or 3.52 HP per cylinder. It can be estimated that 10% to 25% of engine frictional losses occur at the skirt-to-liner interface [14]. Taking the average of 17.5% yields 0.616 HP, or approximately 460 W per cylinder of power loss due to skirt friction. This agrees closely with the value presented in Table 5. The measured FMEP at 3600 RPM was approximately 2.75 bar. Performing the exact same calculation yields approximately 1000 W of power loss at the skirt-to-liner interface, which is again in close agreement with the model prediction. FMEP values of an engine equipped with all APC pistons are to be recorded in the coming phase of the project.

Since the results shown in Table 5 are per cylinder, for a four-cylinder configuration at 3600 RPM, the optimized profile is predicted to reduce the engine average friction power loss by 893 W, or approximately 1.2 HP. The experimental peak horsepower corresponding to the gas pressure data used in the optimization was 155.2 HP. An additional 1.2 HP represents a 0.77% gain in peak horsepower at 3600 RPM, therefore a theoretical 0.77% gain in brake specific fuel consumption. At 2000 RPM the optimized profile yields an additional 203 W, or 0.273 HP for a four-cylinder arrangement. The experimentally measured power at 2000 RPM is approximately 111.25 HP. Therefore, the friction improvements correspond to a 0.25% improvement in power and BSFC at 2000 RPM. It is believed that a more extensive optimization study will yield further performance enhancements. These results are based on geometry alone, without consideration of the surface texture and oil retention improvements of the APC coated piston, or the friction improvements associated with the reduced work on the rings.

## Conclusions and Future Work

This study investigated the geometrical differences between a stock Cummins R2.8 piston and a similar piston that was equipped with a Line2Line abradable powder piston skirt coating. The worn APC piston geometry exhibits a significantly smaller integrated skirt clearance (ISC) than the stock coated piston,

resulting in a significant reduction in piston secondary motion and piston tilt. This improvement offers reduced piston noise, reduced vibration, and improves one mode of piston wear. The effect of this reduction in piston motion on ring groove side wear has also been investigated. The groove side wear results suggest that a reduction in piston secondary motion will also yield a significant reduction in groove side wear, and therefore enhanced ring performance and extended durability. It is also likely that reduced secondary motion will improve the sealing capabilities of the compression rings. This effect will be investigated in the future.

This investigation emphasized solely the macroscopic skirt geometry changes while largely neglecting the effect of surface texture differences on the piston secondary motion and power loss. Chowdhury [6] showed that the worn APC piston skirt houses numerous micron-sized oil retaining pockets. The regions which come in contact with the cylinder liner closely resemble a plateau-honed surface, where the surface topology of the plateau regions is significantly different than that of the pocket regions. Malburg [11] proposed a method of representing a stratified surface (with two different regions of surface texture) by linearizing the bearing area curve to characterize the plateau and pocket regions of a plateau-honed surface. This method essentially splits the surface into two normal distributions; therefore the surface is referred to as “bi-gaussian”. Leefe [12] used this surface modeling technique to derive a bi-gaussian elastic asperity contact model, which was then improved upon by Hu et al [13]. These models account for the reduced contact area resulting from the oil retaining pockets on a plateau-honed surface. The implementation of this model is being investigated, as it provides an improved method of modeling the surface characteristics of the APC piston. Efforts are being made to update the simulation inputs across a range of operating conditions. As detailed experimental information becomes available, the piston temperature distribution, bore expansion, liner temperature, etc. will be updated for a more accurate reflection of the conditions being studied. The improved simulation inputs will also be used to calculate the ISC of both the coated and stock piston at operating temperature. Finally, two additional engine tests are being conducted to investigate the overall performance of an engine equipped with APC pistons and a stock configuration. The post-run geometries of this engine will be analyzed in the current model, and the dynamometer data will be analyzed to study the coating effect on engine friction and resulting improvements in engine fuel consumption.

## References


1. Zhu, Dong & Cheng, Herbert & Arai, Takayuki & Hamai, Kyugo. (1992). A Numerical Analysis for Piston Skirts in Mixed Lubrication—Part I: Basic Modeling. Journal of Tribology. 114. 553. 10.1115/1.2920917.
2. Patir, N., and Cheng, H. S. (January 1, 1978). "An Average Flow Model for Determining Effects of Three-Dimensional Roughness on Partial Hydrodynamic Lubrication." ASME. J. of Lubrication Tech. January 1978; 100(1): 12–17. https://doi.org/10.1115/1.3453103
3. Patir, N., and Cheng, H. S., 1979, “Application of Average Flow Model to Lubrication Between Rough Sliding Surfaces,” J. Lubrication Tech., 101(2), pp. 220–229.
4. Gunelsu, O., and Akalin, O. (January 31, 2014). "The Effects of Piston Skirt Profiles on Secondary Motion and Friction." ASME. J. Eng. Gas

Turbines Power. June 2014; 136(6): 062503. https://doi.org/10.1115/1.4026486

5. Totaro, P., Westerfield, Z., and Tian, T., "Introducing a New Piston Skirt Profile to Reduce Engine Friction," SAE Technical Paper 2016-01-1046, 2016, doi:10.4271/2016-01-1046.

6. Chowdhury, S.S., Fedewa, B., Schock, H., and Suman, A., "Tribological Performance Assessment of Abradable Powder Coated Pistons Considering Piston Skirt Geometry and Surface Topography," SAE Technical Paper 2021-01-1231, 2021, doi:10.4271/2021-01-1231.

7. Greenwood, James & Tripp, J. (1970). The Contact of Two Nominally Flat Rough Surfaces. Archive: Proceedings of The Institution of Mechanical Engineers 1847-1982 (vols 1-196). 185. 625-634. 10.1243/PIME_PROC_1970_185_069_02.

8. Panayi, Andreas Petrou. "Numerical Models for the Assessment of the Cylinder-Kit Performance of Four-Stroke Internal Combustion Engines." 2009.
9. Arcoumanis, C., et al. "Mixed Lubrication Modelling of Newtonian and Shear Thinning Liquids in a Piston-Ring Configuration." *SAE Technical Paper Series*, 1997, https://doi.org/10.4271/972924.

10. Archard, J. F., 1953, "Contact and Rubbing of Flat Surfaces," Journal of Applied Physics, Vol. 24, pp. 981—988

11. Mark C. Malburg, Jay Raja, David J. Whitehouse, Characterization of Surface Texture Generated by Plateau Honing Process,CIRP Annals,Volume 42, Issue 1,1993,Pages 637-639

12. Leefe, S. E., 1998, "'Bi-Gaussian' Representation of Worn Surface Topography in Elastic Contact Problems," Tribol. Ser., 34, pp. 281–290.

13. Hu, S., Brunetiere, N., Huang, W., Liu, X., and Wang, Y. (January 10, 2017). "Stratified Revised Asperity Contact Model for Worn Surfaces." ASME. J. Tribol. March 2017; 139(2): 021403.

14. Cheng, Chao, and Harold Schock. "Engine Friction Measurement with Floating Cylinder Liner." East Lansing , Michigan .

15. Pistons and Engine Testing. Springer Fachmedien Wiesbaden, Imprint: Springer Vieweg, 2016.

16. Ayatollahi, Majid R. & Mohammadi, F. & Chamani, Hamidreza. (2011). Thermo-Mechanical Fatigue Life Assessment of a Diesel Engine Piston. International Journal of Automotive Engineering. 1. 256-266.

17. Lu, Yaohui & Zhang, Xing & Xiang, Penglin & Dong, Dawei. (2016). Analysis of Thermal Temperature Fields and Thermal Stress under Steady Temperature field of Diesel Engine Piston. Applied Thermal Engineering. 113. 10.1016/j.applthermaleng.2016.11.070.

## Acknowledgments

This work is supported by SBIR Phase II, Department of Defense Contract No. W56HZV-20- C-0010- "High Temperature Wear Coatings for Improving High Output Military Diesel Engine Performance and Durability"

## Definitions

APC – Abradable powder coated

ISC – Integrated skirt clearance

CASE – Cylinder-Kit Analysis System for Engines.

## Appendix A: Mesh Sensitivity Study

To demonstrate the effect of varying the piston mesh density on both the static FEA and piston dynamics results, a brief mesh sensitivity study has been completed. Two simulations were carried out while only varying the piston mesh density. The first simulation utilized the coarse mesh employed in the optimization study, while the second simulation used a refined mesh. The mesh parameters and simulation results are shown in the following table figures.

| Mesh | Number of Nodes | Number of Elements | Size (mm) |
|---|---|---|---|
| **Coarse** | 3457 | 16373 | Skirt: 6<br>Else: 8 |
| **Fine** | 22029 | 104228 | 2.5 |

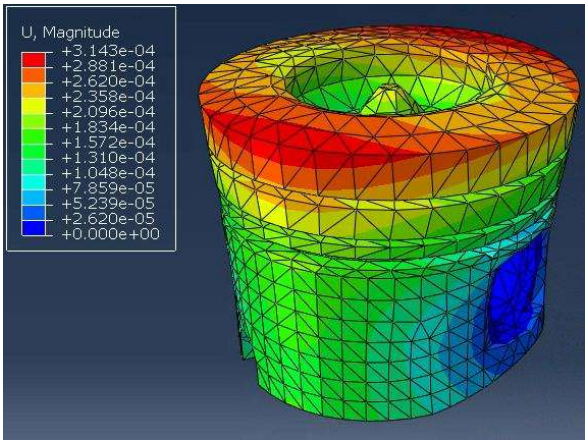


**Figure 23. Coarse Mesh Thermal Deformation (m)**

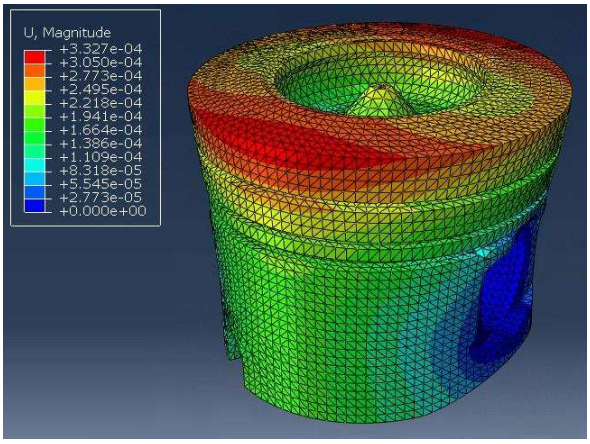


**Figure 24. Fine Mesh Thermal Deformation (m)**

There are limitations on the number of nodes CASE-PISTON can accept due to the limited size of several arrays. Since the static FEA results are not significantly sensitive to the mesh density, the mesh density was refined on the skirt while leaving the mesh relatively coarse elsewhere. This was done to investigate the effects of the mesh size on the piston dynamics results. The mesh parameters and

simulation results are shown in the following table and figures.

| Mesh | Number of Nodes on Thrust | Number of Nodes on Anti - Thrust |
|---|---|---|
| **Coarse** | 152 | 147 |
| **Fine** | 462 | 455 |

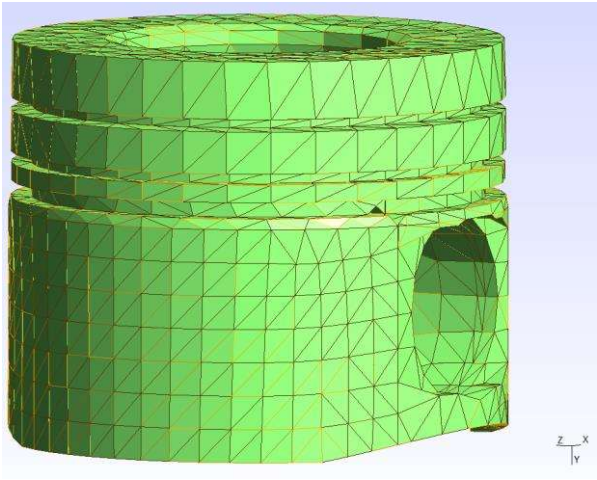

**Figure 25. Coarse Skirt Mesh**

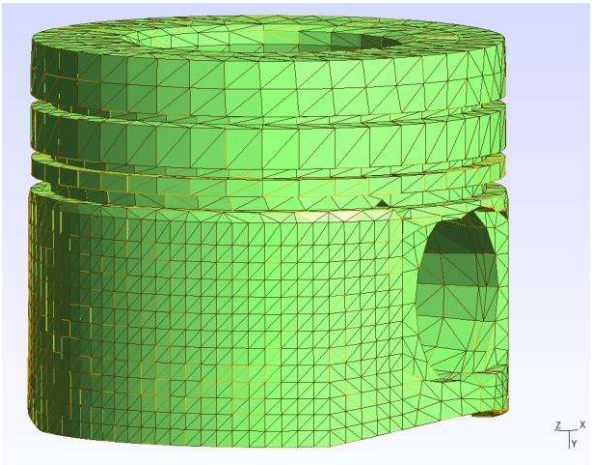

**Figure 26. Refined Skirt Mesh**

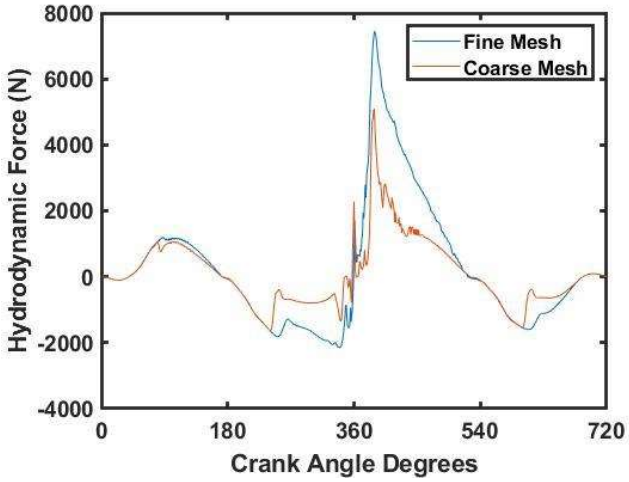


**Figure 27. Mesh Study Hydrodynamic Force**

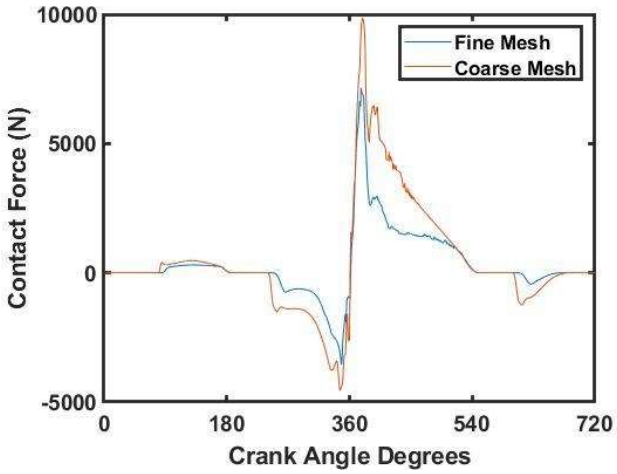


**Figure 28. Mesh Study Contact Force**

While the piston performance prediction is influenced by the skirt mesh density, the coarse mesh results are believed to be sufficient for the comparative nature of the optimization study.